CHEMISTRY
A EUROPEAN JOURNAL

DOI: 10.1002/chem.200601072

From Trifluoroacetate Complex Precursors to Monodisperse Rare-Earth Fluoride and Oxyfluoride Nanocrystals with Diverse Shapes through Controlled Fluorination in Solution Phase

**Xiao Sun,[a] Ya-Wen Zhang,*[a] Ya-Ping Du,[a] Zheng-Guang Yan,[a] Rui Si,[a]
Li-Ping You,[b] and Chun-Hua Yan*[a]**

Abstract: We report the first systematic synthesis of monodisperse rare-earth (RE = La to Lu, Y) fluoride and oxyfluoride nanocrystals with diverse shapes (trigonal REF_3 triangular, truncated-triangular, hexagonal, and polygonal nanoplates; orthorhombic REF_3 quadrilateral and zigzag-shaped nanoplates; cubic REOF nanopolyhedra and nanorods) from single-source precursors (SSP) of $[RE(CF_3COO)_3]$ through controlled fluorination in oleic acid (OA)/oleylamine (OM)/1-octadecene (ODE). To selectively obtain REF_3 or REOF nanocrystals, the fluorination of the RE−O bond to the RE−F bond at the nucleation stage was controlled by finely tuning the ratio of OA/ODE or OA/OM, and the reaction temperature. For phase-pure REF_3 or REOF naocrystals, their shape-selective syntheses could be realized by further modifying the reaction conditions. The two-dimensional growth of the REF_3 nanoplates and the one-dimensional growth of the REOF nanorods were likely due to the selective adsorption of the capping ligands on specific crystal planes of the nanocrystals. Those well-shaped nanocrystals with diverse geometric symmetries (such as D_{3h}, D_{6h}, C_{2h}, O_h, and D_{nh}) displayed a remarkable capability to form self-assembled superlattices. By manipulating the solvent–substrate combination, the plate-shaped REF_3 nanocrystals could form highly ordered nanoarrays by means of either the face-to-face formation or the edge-to-edge formation. By using this SSP strategy, we also obtained high-quality LaF_3:Eu and LaF_3:Eu/LaF_3 triangular nanoplates that showed photoluminescent red emissions of Eu^{3+} ions sensitive to the surface effect.

Keywords: fluorescence · nanostructures · rare-earth fluorides · self-assembly · synthetic methods

Introduction

The synthesis of colloidal nanocrystals (sometimes called "artificial atoms") with controlled shape, size, composition, phase, and surface state endows such materials with unique optical, electronic, magnetic, and catalytic properties, which are fundamentally important and technologically useful.[1–3] The integration of size-/shape-dependent properties and ease of fabrication, processing, and self-assembly enables such nanocrystals to act as ideal building blocks for materials or nanodevices with designed functions.[1] Modification of their surfaces with capping ligands allows them to readily form two- and three-dimensional superstructures and/or superlattices composed of single component or binary component nanoparticles on substrates through spontaneous organization. Such procedures have received broad interest from theoretical simulation to experimental fabrication and microcosmic explanation of the mono- or multiple-layer patterns.[2] Therefore, the synthesis of diverse high-quality inorganic nanocrystals with tunable shape and size, and the exploration of their size-/shape-control and self-assembly principles, have become two of the most challenging issues faced by chemists.[1–3] So far, the nonhydrolytic approach by using either multiple- or single-source precursors (SSP) in the solution phase offers convenient and reproducible routes for

---

[a] X. Sun, Prof. Dr. Y.-W. Zhang, Y.-P. Du, Dr. Z.-G. Yan, Dr. R. Si,
Prof. Dr. C.-H. Yan
Beijing National Laboratory for Molecular Sciences
State Key Laboratory of Rare Earth Materials Chemistry
and Applications
PKU-HKU Joint Laboratory in Rare Earth Materials
and Bioinorganic Chemistry
Peking University, Beijing 100871 (P.R. China)
Fax: (+86) 10-6275-4179
E-mail: yan@pku.edu.cn
ywzhang@pku.edu.cn

[b] Prof. Dr. L.-P. You
Electron Microscopy Laboratory
Peking University, Beijing 100871 (China)

Supporting information for this article is available on the WWW under http://www.chemistry.org or from the author.

the fabrication of such colloid nanocrystals.[3,4] In this approach, the identification of suitable molecular precursors, the regulation of solvent-coordinating capability, and the balance of the nucleation and growth stages are the three requisites for obtaining high-quality products.

Recently, nanocrystals of dispersible rare-earth (RE) compounds (such as oxides,[5] phosphates,[6] vanadates,[7] sulfides,[8] and fluorides[9]) have become of rapidly growing importance due to their promising applications in phosphors, magnets, catalysts, and biolabels. Rare-earth fluoride (such as LaF_3, CeF_3, GdF_3, YF_3, LaF_3:Eu/Er/Nd/Ho, CeF_3:Tb, GdF_3/LaF_3, $NaREF_4$, $NaYF_4$:Yb,Er/Tm) nanocrystals have drawn particular attention owing to their potential uses in lighting and displays, optical amplifies, lasers, bioprobes, and NMR and MRI relaxation agents.[9] As far as we know, the REF_3 nanocrystals are generally prepared by some limited, wet chemical routes involving modified precipitation,[9a,g,h,j] hydrothermal treatment,[9e] microemulsion,[9f] and polyol[9i] methods, which are based on the liquid precipitation reaction between the rare-earth nitrates/chlorides and NaF/NH_4F. In contrast, the REOF nanocrystals are made by a mechanochemical processing in air, by using rare-earth oxide and polytetrafluoroethylene as the solid reactants.[10] To date, there have been a few reports of the synthesis of dispersible REF_3 nanocrystals, but not of REOF ones.[9a,c,j] It still remains a challenge to develop a new route towards a general synthesis of high-quality REF_3 and REOF nanocrystals.

We recently reported the synthesis of single-crystalline and monodisperse LaF_3 triangular nanoplates by thermolysis of $[La(CF_3COO)_3]$ in oleic acid/1-octadecene.[9c] Here, we present the systematic synthesis of high-quality REF_3 and REOF (RE = La to Lu, Y) nanocrystals with diverse shapes by using the thermolysis of $[RE(CF_3COO)_3]$ in oleic acid/oleylamine/1-octadecene. With this unique single-source precursor (SSP) method, we prepared triangular, truncated-triangular, hexagonal, and polygonal nanoplates of trigonal REF_3, quadrilateral, and zigzag-shaped nanoplates of orthorhombic REF_3, and nanopolyhedra and nanorods of cubic REOF, by controlling the fluorination of the RE−O bond to the RE−F bond at the nucleation stage, and by finely tuning the nanocrystal-growth kinetics in the hot solvents. We also obtained LaF_3:Eu and LaF_3:Eu/LaF_3 triangular nanoplates, which showed interesting photoluminescent (PL) properties related to the surface effect. More importantly, the as-obtained REF_3 and REOF nanocrystals exhibited an intriguing self-assembly capability to form superlattice structures.

Results and Discussion

Characterization of REF_3 and REOF (RE = La to Lu, Y) nanocrystals

Trigonal REF_3 (RE = La to Ho) nanocrystals: Figure 1 and Figure S1 show that the peaks for each sample of REF_3 (RE = La to Ho) nanocrystals can be readily indexed to a pure trigonal phase (space group: $P\bar{3}c1$). From Figure 1, the calculated lattice constants are as follows: a = 7.171 and c = 7.176 Å for CeF_3 (JCPDS: 38–452), a = 7.121 and c = 6.988 Å for NdF_3 (JCPDS: 9–416), a = 6.98 and c = 6.993 Å for SmF_3 (JCPDS: 12–792), and a = 6.907 and c = 6.971 Å for GdF_3.[12] For the as-obtained trigonal REF_3 nanocrystals, the plots of their cell volumes against the number of REF_3 molecules are in agreement with the lanthanide contraction (Figure S2). The broadening of the diffraction peaks distinctly reveals the nanocrystalline nature of the samples.

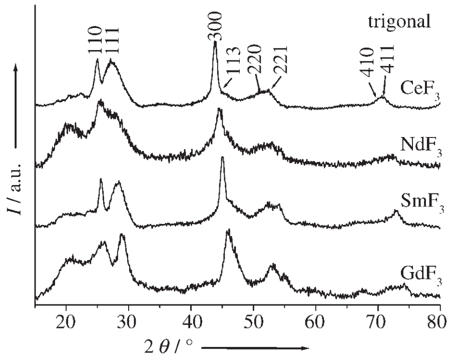

Figure 1. XRD patterns of trigonal REF_3 (RE = Ce, Nd, Sm, Gd) nanocrystals.

The TEM measurements reveal that all the as-obtained trigonal REF_3 nanocrystals show a platelike shape, that is, triangular nanoplates for LaF_3 and CeF_3, truncated-triangular nanoplates for PrF_3 and NdF_3, hexagonal nanoplates for SmF_3 and EuF_3, and polygonal nanoplates for those from GdF_3 to HoF_3. Figure 2a depicts the TEM image of the CeF_3 triangular nanoplates of size (1.4 ± 0.2) nm × (14.4 ± 0.5) nm. The CeF_3 nanocrystals formed highly aligned triangular nanoplate arrays on the TEM grid, either standing on the edge or lying flat on the face, revealing the high size uniformity of the nanocrystals capped by oleate ligands. The HRTEM images (insets in Figure 2a) demonstrate that the CeF_3 nanocrystals are single-crystalline, equilaterally-triangular nanoplates, enclosed by the {0001} and {11$\bar{2}$0} facets. The side surface of the nanoplates comprises only four layers of the (0002) facet. Under the same synthetic conditions as those for preparing CeF_3 nanoplates, we also obtained high-quality LaF_3 triangular nanoplates of size (2.0 ± 0.1) nm × (16.0 ± 0.4) nm.[9c] The triangular nanoplates could spontaneously organize into two types of superlattices (edge-to-edge and face-to-face) on a large area by manipulating the solvent–substrate combination.[9c] The deposition of a NdF_3 nanocrystal dispersion in toluene/hexane (v/v = 1:3) led to the highly ordered alignment of these truncated-triangular nanoplates, either lying flat on the face (Figure 2b) or standing on the edge (Figure 2c) on the same TEM grid. The NdF_3 nanoplates are highly uniform, and are single-crystalline showing an interplanar spacing of 0.33 nm of {11$\bar{2}$0} facets in the HRTEM image (Figure 2d). The nanoplates have two categories of edge length: 8.0 ± 1.0 nm (long edge) and 2.9 ± 0.5 nm (short edge). The side plane of

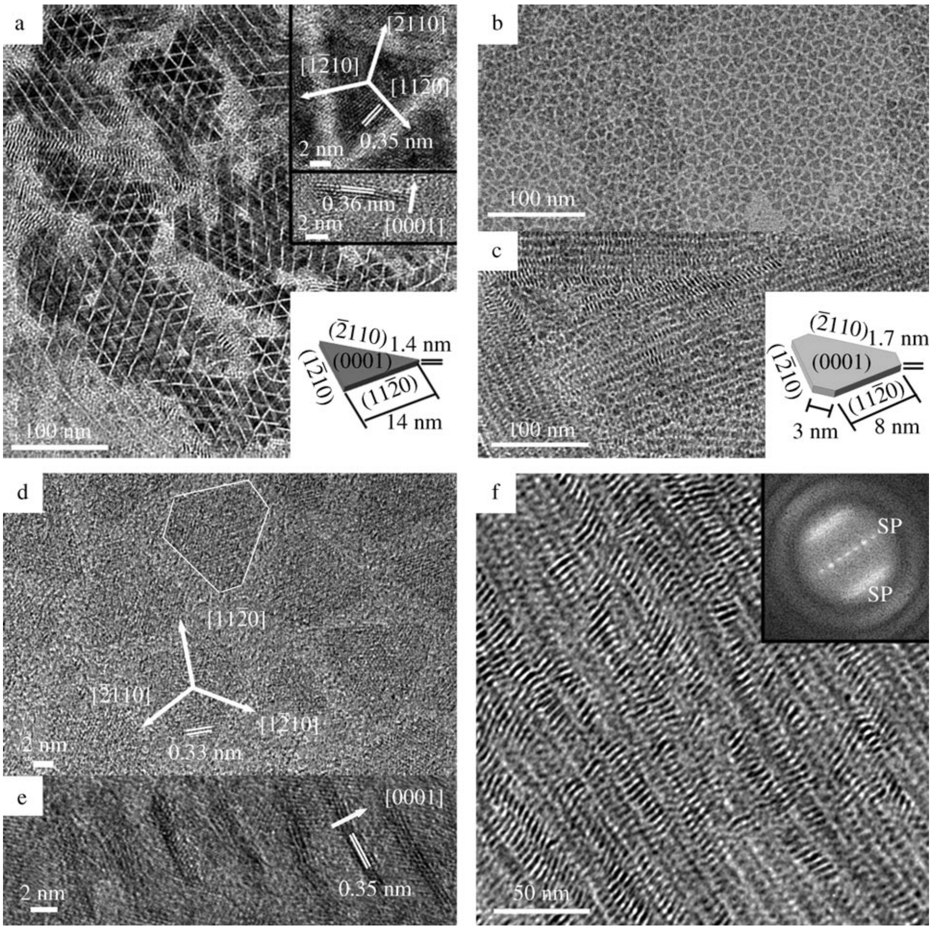

Figure 2. a) TEM and HRTEM (upper insets) images of CeF_3 triangular nanoplates, the lower inset is a schematic diagram of a triangular nanoplate. TEM images of NdF_3 truncated-triangular nanoplates b) lying flat on the face and c) standing on the edge (inset is a schematic diagram of a truncated-triangular nanoplate). HRTEM images of an aligned NdF_3 truncated-triangular nanoplate array d) lying flat on the face and e) standing on the edge. f) TEM image of the face-to-face superlattices (SP) of PrF_3 truncated-triangular nanoplates, inset shows results of a FFT analysis.

the standing aligned nanoplates comprises five (0002) layers with an interplanar spacing of 0.35 nm (Figure 2e), and shows a thickness of 1.7 ± 0.3 nm. The interparticle distance is approximately 2.4 nm, which seems to fit the thickness of one monolayer of the capping oleates. The HRTEM images given in Figure 2d,e show that the {0001} and $\{11\bar{2}0\}$ facets enclose the NdF_3 nanoplates (inset in Figure 2c). Under the same synthetic conditions as those for obtaining NdF_3 nanoplates, PrF_3 truncated-triangular nanoplates of size $(1.8 \pm 0.2)\,\text{nm} \times (5.2 \pm 0.7)\,\text{nm} \times (8.5 \pm 1.1)\,\text{nm}$ were also prepared. Figure 2f shows the highly ordered nanoarrays of PrF_3 nanoplates in the face-to-face formation along the [0001] direction on the TEM grid, as deposited from the high-concentration nanoplate dispersion in toluene/hexane/ethanol. The fast Fourier transform (FFT) analysis (inset in Figure 2f) reveals two sets of spots, representing a periodicity length of 13.9 nm (inter-ribbon distance) and 4.0 nm (interparticle distance).

Figure 3a shows the highly ordered alignment of the SmF_3 hexagonal nanoplates either lying flat on the face or standing on the edge, as deposited from the nanocrystal dispersion in toluene/hexane (v/v = 1:3). HRTEM images (insets in Figure 3a, together with Figure 3b,c) disclose that the SmF_3 nanoplates are highly uniform, with six equilateral edges of length 12.7 ± 0.5 nm, and have a thickness of 1.8 ± 0.2 nm. From the insets in Figure 3a, an interplanar spacing of 0.20 nm ascribed to the (300) facet is observable on the top surface of the nanoplate, revealing its single-crystalline nature. The standing nanoplate shows a side plane composed of five (0002) layers with an interplanar spacing of 0.35 nm. Consequently, the enclosing crystal planes determined for the hexagonal nanoplates are the {0001} and $\{11\bar{2}0\}$ facets (see the upper diagram in Figure 3d). From Figure 3a, we can also see that the lying nanoplates show a predominately hexagonally close-packed (*hcp*) superlattice. Interestingly, several wheel-like nanoarrays consisting of the lying nanoplates were also observed (upper highlighted circle in Figure 3a). The HRTEM image (Figure 3b) reveals that the wheel-like nanoarray has two parts: a core composed of the lying nanoplates, and a ring enclosing the core composed of obliquely lying nanoplates (schematically depicted in the lower diagram of Figure 3d). To our knowledge, such a wheel-like nanocrystal superstructure has been reported only once.[2e] Figure 3e displays the *hcp* superlattice of the SmF_3 hexagonal nanoplates in the edge-to-edge formation on the TEM grid, as deposited from their low-concentration dispersion in toluene/hexane (v/v = 1:3). The FFT analysis (inset in Figure 3e) reveals six-fold symmetric spots, representing a periodicity length of 2.9 nm (interparticle distance). Figure 3f exhibits the highly ordered nanoarrays of the SmF_3 nanoplates in the face-to-face formation along the [0001] direction on the TEM grid, as deposited from their high-concentration dispersion in toluene/hexane/ethanol. Under the same synthetic conditions as those for obtaining the SmF_3 nanoplates, $(2.2 \pm 0.2)\,\text{nm} \times (11.5 \pm 1.0)\,\text{nm}$ EuF_3 hexagonal nanoplates were synthesized, which also exhibited highly ordered alignment on the TEM grid (Figure 3g).

In contrast to the REF_3 nanoplates from La to Eu, the geometrical shapes of the top surfaces for those from Gd to

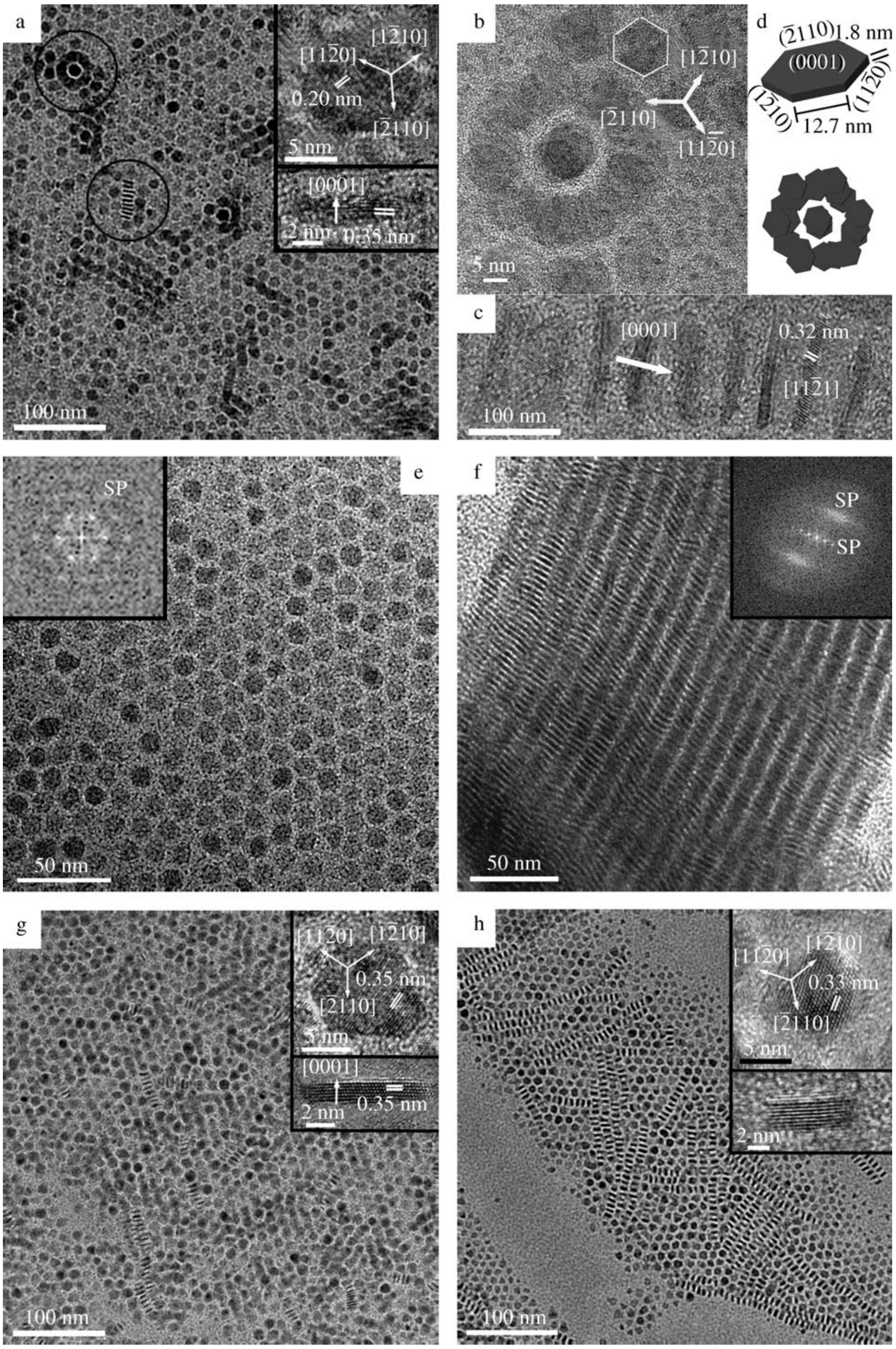

Figure 3. a) TEM and HRTEM (insets) images of SmF_3 hexagonal nanoplates. b) and c) show the HRTEM images of a wheel-like array of the nanoplate lying flat on the face, and an aligned array of the nanoplate standing on the edge, respectively (as taken from the highlighted circles in (a)). d) Schematic diagrams of SmF_3 hexagonal nanoplate and its wheel-like array. TEM images of e) the edge-to-edge and f) face-to-face superlattices (SP) of SmF_3 hexagonal nanoplates, insets show results of FFT analyses. TEM and HRTEM (insets) images of g) EuF_3 hexagonal and h) GdF_3 polygonal nanoplates.

Ho are quite complex, for example, hexagonal, triangular, and quadrangular. (Figure 3h and Figure S3). Figure 3h shows the TEM image of the GdF_3 polygonal nanoplates. These formed nanoarrays either lying flat on the face or standing on the edge, and have an estimated size of 3.0 nm × 8.7 nm. From the insets in Figure 3h, the presence of GdF_3 hexagonal nanoplates can be confirmed.

Orthorhombic REF_3 (RE = Gd to Lu, Y) nanocrystals: The broadened diffraction peaks shown in Figure 4 and Figure S4 reveal the formation of orthorhombic REF_3 (RE = Gd to Lu, Y) nanocrystals (space group: *Pnma*). From Figure 4, the calculated lattice constants are as follows: $a = 6.552$, $b = 7.07$, and $c = 4.373$ Å for GdF_3 (JCPDS: 12–788), $a = 6.40$, $b = 6.9$, and $c = 4.46$ Å for HoF_3 (JCPDS: 23–284), $a = 6.399$, $b = 6.923$, and $c = 4.365$ Å for YF_3 (JCPDS: 32–1431), and $a = 6.417$, $b = 6.8$, and $c = 4.345$ Å for YbF_3 (JCPDS: 32–1418).[12] As expected from the lanthanide contraction, the orthorhombic lattice volume has a decreasing tendency from GdF_3 to LuF_3 (Figure S2).

TEM characterization demonstrated that all the as-obtained orthorhombic REF_3 nanocrystals display a platelike shape (Figure 5 and Figure S5), that is, zigzag-shaped nanoplates for GdF_3, and quadrilateral nanoplates for REF_3 (RE = Tb to Lu, Y). Figure 5a depicts the nanoarrays formed by the GdF_3 zigzag-shaped nanoplates either standing on the edge or lying flat on the face. The long edges of the top surface for the GdF_3 nanoplates clearly appear in zigzag form (Figure 5a), and have a length of approximately 51 nm. The length of the short edge of the top surface of the nanoplates is around 12 nm. Also from Figure 5b, the interplanar distances of 0.20 nm ascribed to the (002) facet and 0.33 nm attributed to the (200) facet are observed on the top surface of the nanoplate. Figure 5c shows the HRTEM image of an aligned GdF_3 nanoplate array standing on the edge. The large side surface of the nanoplates comprises six (020) layers, and shows a thickness of approximately 2.1 nm. Figure 5d exhibits the two-di-

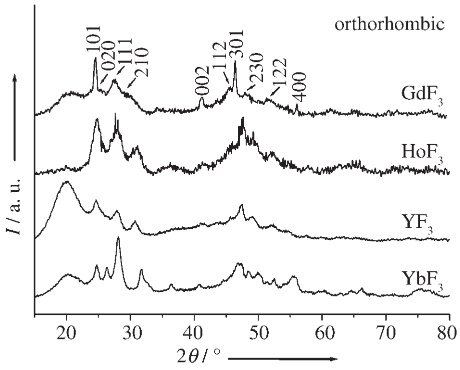

Figure 4. XRD patterns of orthorhombic REF$_3$ (RE = Gd, Ho, Y, Yb) nanocrystals.

mensionally ordered arrangement of YF$_3$ nanoplates lying flat on the face, as deposited from the nanocrystal dispersion in toluene/hexane (v/v = 1:3). The top surface of the YF$_3$ nanoplates is of size (8.3 ± 1.0) nm × (10.4 ± 1.2) nm, on which the interplanar spacing of 0.35 nm ascribed to the (101) facet was identified (inset in Figure 5d). As the YF$_3$ nanoplates were deposited on the TEM grid from their dispersion in toluene/hexane/ethanol, they could be aligned in the face-to-face formation (Figure 5e). The side surface of the nanoplates comprises nine (020) layers, showing a thickness of approximately 3 nm (inset in Figure 5e). Together, the {010} and {101} facets are determined to enclose the quadrilateral nanoplates. Figure 5f,g show the TEM images of quadrilateral HoF$_3$ and YbF$_3$ nanoplates, respectively, whose top surfaces are of size (8.1 ± 0.6) nm × (9.6 ± 0.4) nm and (12.8 ± 2.6) nm × (16.3 ± 4.2) nm, respectively.

Cubic REOF (RE = La to Lu, Y) nanocrystals: The X-ray diffraction (XRD) patterns shown in Figure 6 and Figure S6 reveal cubic REOF (space group: $Fm\bar{3}m$) nanocrystals along the whole rare-earth series. The calculated lattice constants are 5.505 Å for LuF$_3$, 5.49 Å for GdF$_3$, 5.615 Å for SmF$_3$, and 5.803 Å for CeF$_3$ (JCPDS: 22–168). The variation of cubic lattice volume along the rare-earth series basically agrees with the lanthanide contraction (Figure S2) and the result reported by Müller and Petzel.[13]

The as-synthesized cubic REOF nanocrystals display two types of shape; nanopolyhedron shape for the whole REOF series, and nanorod shape for EuOF and GdOF. From Figure 7 and Figure S7, it is noted that the cubic REOF nanocrystals are highly dispersed, and exhibit an intriguing two-dimensionally ordered arrangement, indicative of the retention of capping ligands on the nanocrystal surfaces, which was confirmed by ^{1}H NMR and FTIR measurements (Figure S8). The strong peaks at 2850 and 2920 cm^{-1} and middle strong peak at 3315 cm^{-1} in FTIR spectra are the characteristics of acyclic C−H stretch and aliphatic amine N−H stretch, respectively, a weak vinyl C−H stretch located at 3003 cm^{-1} demonstrates the presence of oleic acid ligands on the nanocrystal surface.[14] However, there is no obvious peak at 1710 cm^{-1}, indicative of no trace amounts of free oleic acid on the surface. The moderately strong carbonyl-stretch peaks at 1553 and 1447 cm^{-1} are assigned to the carboxylate (COO$^-$) stretch. The interplanar distance of 0.26 nm ascribed to the (020) facet is observed in the upper HRTEM inset in Figure 7a, revealing that the LuF$_3$ nanocrystals are of truncated-octahedron shape enclosed by the {111} and {100} facets (schematically shown in the lower inset of Figure 7a). The LuF$_3$ nanopolyhedra have a size of 8.5 ± 0.5 nm. Figure 7b shows the formation of highly uniform GdOF nanorods of size (3.4 ± 0.4) nm × (9.8 ± 1.3) nm. The HRTEM image (inset in Figure 7b) displays the interplanar distances of 0.28 and 0.32 nm attributed to the (200) facet and (111) facet, respectively, suggesting that the preferred growth direction of the nanorods is along the [100] direction. Figure 7c,d exhibits the two-dimensional superlattice composed of SmOF and CeOF nanopolyhedra of size 4.1 ± 0.4 and 4.5 ± 0.4 nm, respectively.

Formation of REF$_3$ and REOF nanocrystals: REF$_3$ has two polymorphs at room temperature: trigonal (tysonite LaF$_3$ type shown in Figure S9a; space group: $P\bar{3}c1$) and orthorhombic (β-YF$_3$ type shown in Figure S9b; space group: *Pnma*).[12] Light REF$_3$ (RE = La to Nd) and heavy REF$_3$ (RE = Dy to Lu, Y) existed only in the trigonal and orthorhombic forms, respectively, whereas middle REF$_3$ (RE = Sm to Tb) could be prepared as either the trigonal or orthorhombic form.[12b] The trigonal↔orthorhombic transition is of first-order character. The stoichiometric REOF usually appears in two modifications: low-temperature β form (rhombohedral; space group: $R\bar{3}m$) and high-temperature α form (cubic structure shown in Figure S9c; space group: $Fm\bar{3}m$).[13] For our REF$_3$ nanocrystals obtained in this work, those from La to Eu had only the trigonal structure, those from Gd to Ho exhibited dimorphism (trigonal and orthorhombic), and those from Er to Lu, including Y, were of only orthorhombic phase. All the as-prepared REOF nanocrystals took the high-temperature α form. The atomic ratios of fluorine to metal in the nanocrystals were determined by X-ray photoelectron spectroscopy (XPS), confirming the formation of pure REF$_3$ or REOF (Figure S10). Serial experiments revealed that the formation of high-quality REF$_3$ and REOF nanocrystals of diverse shapes with different geometric symmetries was realized by a homogeneous nucleation through a controlled fluorination of the RE−O bond to the RE−F bond in oleic acid (OA)/oleylamine (OM)/1-octadecene (ODE), by using F$^-$ ions produced from the cleavage of the C−F bond of the trifluoroacetate ligands during the thermolysis of [RE(CF$_3$COO)$_3$], together with a sustained balance between the nucleation and growth stages (Scheme 1). The nature of the rare-earth element, the solvent composition, as well as the reaction temperature, have been shown to play crucial roles in the phase-selective growth of high-quality REF$_3$ or REOF nanocrystals through the controlled fluorination in solution phase.

Nucleation: Based on the phase compositions of the condition-dependent synthetic products analyzed by the XRD

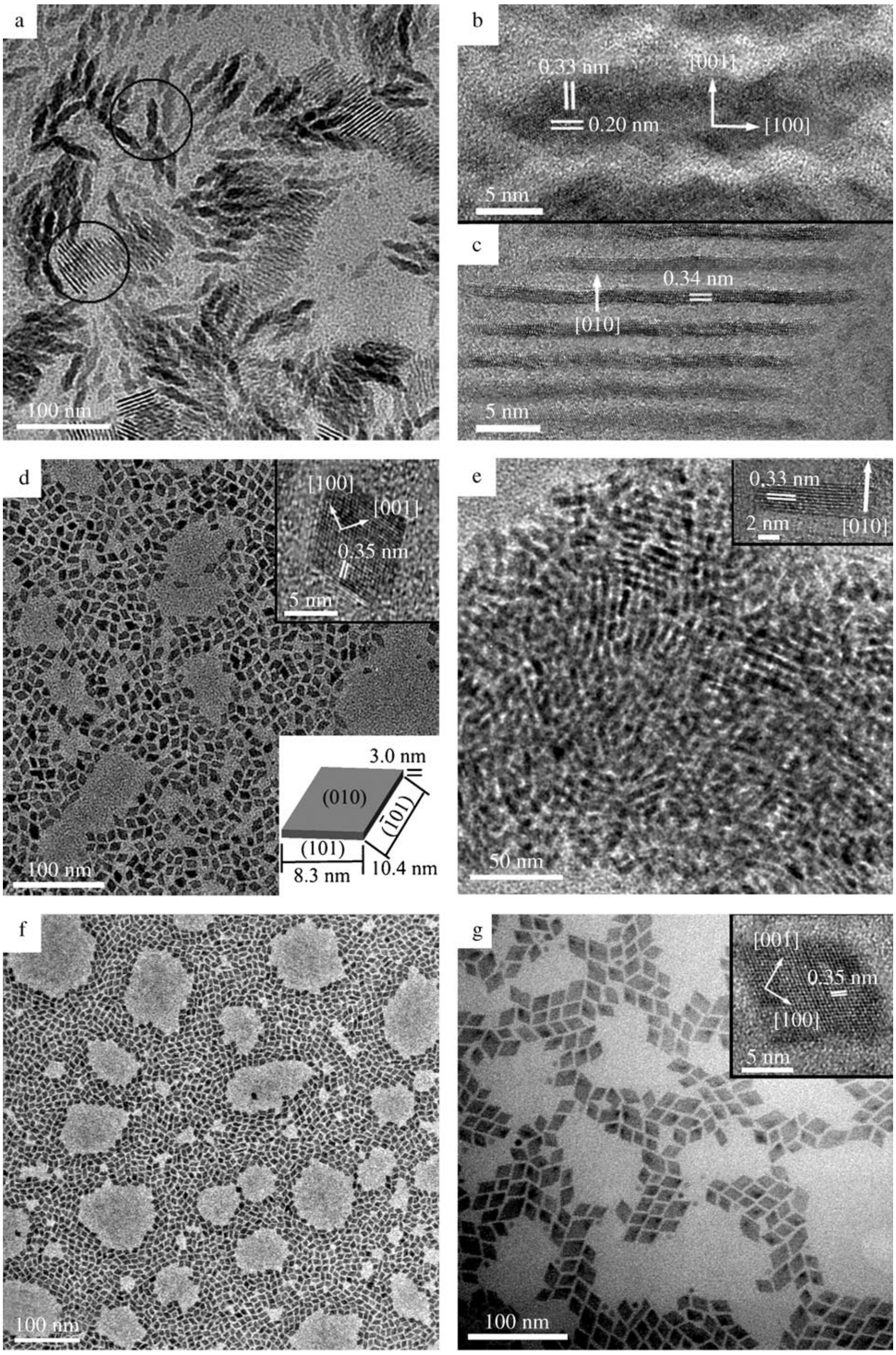

Figure 5. a) TEM image of GdF_3 zigzag-shaped nanoplates. b) and c) show HRTEM images of a GdF_3 nanoplate lying flat on the face, and its nanoplate array standing on the edge, respectively (as taken from the highlighted circles in (a)). d) TEM and HRTEM (upper inset) images of YF_3 quadrilateral nanoplates lying flat on the face, the lower inset shows a schematic diagram of a quadrilateral nanoplate. e) TEM and HRTEM images (inset) of YF_3 quadrilateral nanoplates standing on the edge. TEM images of f) HoF_3 and g) YbF_3 quadrilateral nanoplates lying flat on the face (inset is the HRTEM image of a YbF_3 nanoplate).

method (Tables S1–S4), we could retrieve the nature (REF_3 or REOF) of the nuclei involved in the present nanocrystal synthesis. The thermolysis temperature of $[RE(CF_3COO)_3]$ in OA/OM/ODE was observed to increase gradually across the rare-earth series from approximately 280 °C for La to approximately 310 °C for Lu. As the solution containing $[RE(CF_3COO)_3]$ was rapidly heated to its thermolysis temperature under an Ar atmosphere, some tiny gas bubbles were emitted promptly from the reaction system, which implied an instant decomposition of the precursor and a simultaneous formation of homogeneous rare-earth nuclei.[9c,11] For example, as determined by using a gas chromatograph-mass spectrometer, the mass peaks of 44, 51, and 69 attributed to CO_2, CF_2H^+ and CF_3^+, respectively, were identified on the mass spectrum of the low-molecular-weight components, as $[Ho(CF_3COO)_3]$ in OA/ODE (1:1) was heated quickly to 280 °C (Figure S11). As a result, the major components of the gas bubbles were concluded to be CO_2 and fluorinated/oxyfluorinated carbon species, as in the case of the pyrolysis of the $[Nd(CF_3COO)_3]$ powder in a muffle furnace.[11] Originally, both in solid and in solution phase, rare-earth ions were coordinated by oxygen atoms, therefore, it is rational that the retention of the RE−O bond would occur in the initial nucleation stage during the thermolysis of $[RE(CF_3COO)_3]$ in OA/OM/ODE (Scheme 1). At the same time, highly reactive F^- ions were released due to the breaking of the C−F bond in CF_3COO^-. Consequently, the fluorination of the RE−O bond to the RE−F bond would inevitably take place, and the subsequent replacement of the RE−O bond with the RE−F bond would lead to the formation of REOF and REF_3 nuclei in turn, which depended upon the thermolysis conditions of the trifluoroacetate complexes.

Experimentally, in OA/ODE, we found that only REF_3 nuclei were formed for the rare earths from La to Eu, thanks to the relatively high basicity of their oxides (Tables S1–S4). However, REF_3 and/or REOF nuclei could be

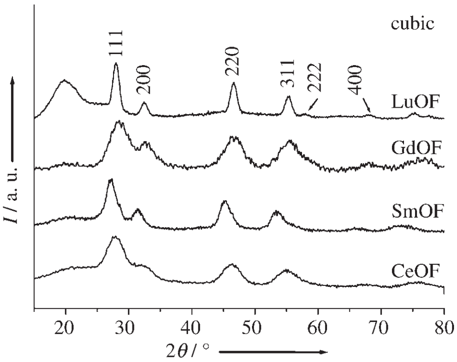

Figure 6. XRD patterns of cubic REOF (RE = Ce, Sm, Gd, Lu) nanocrystals.

formed for the rare earths from Gd to Lu, including Y. The higher OA/ODE ratio and the reaction temperature either close to the decomposition temperature of the precursors or higher than 320 °C appeared to favor the formation of REOF nuclei. By adding OM to OA, the fluorination interaction was considerably weakened owing to the stronger fluorophilicity of OM, which is more basic than rare-earth oxides. This result strongly suggests that oleylamine ligand is a delicate buffer of F^- ions, allowing the regulated fluorination to selectively form REOF nuclei. As a result, REOF nuclei could also be formed for the rare earths from La to Eu under these conditions (Table S2). Naturally, the lighter the rare earth, the more OM it required, owing to the fact that the basicity of the rare-earth oxide gradually decreases along the rare-earth series. With the nuclei of REF_3 and REOF formed through the controlled fluorination, their high-quality nanocrystals could be prepared by maintaining the balance between nucleation and growth stages.

Nanocrystal growth: For obtaining high-quality REF_3 and REOF nanocrystals, we found that the solvent composition was likely the key factor among the synthetic parameters for a given rare-earth element. In OA/ODE solutions, the higher OA/ODE ratio usually produced highly soluble but less uniform REF_3 nanocrystals. In contrast, the lower OA/ODE ratio yielded less soluble, more aggregated, and poorly shaped crystals.[9c] Therefore, high-quality trigonal REF_3 (RE = La to Ho) or orthorhombic REF_3 (RE = Gd, Tb, Y, Tm, Yb, Lu) nanocrystals were generally obtained at OA/ODE = 1:1 (Table S1) at temperatures ranging from 280 to 320 °C. However, it was difficult to obtain high-quality orthorhombic DyF_3, HoF_3, and ErF_3 nanocrystals in OA/ODE, probably due to the ease of their trigonal↔orthorhombic transition under these conditions. The addition of a substantial amount of OM into OA made their orthorhombic phase more stable, and led to the formation of the high-quality orthorhombic nanocrystals at OA/OM = 5:3 (Table S1). By precisely tuning the amount of OM, high-quality REOF (RE = La to Ho, Y) nanocrystals could be obtained. In contrast, those from Er to Lu were synthesized at OA/ODE = 1:1 in the absence of OM (Table S2).

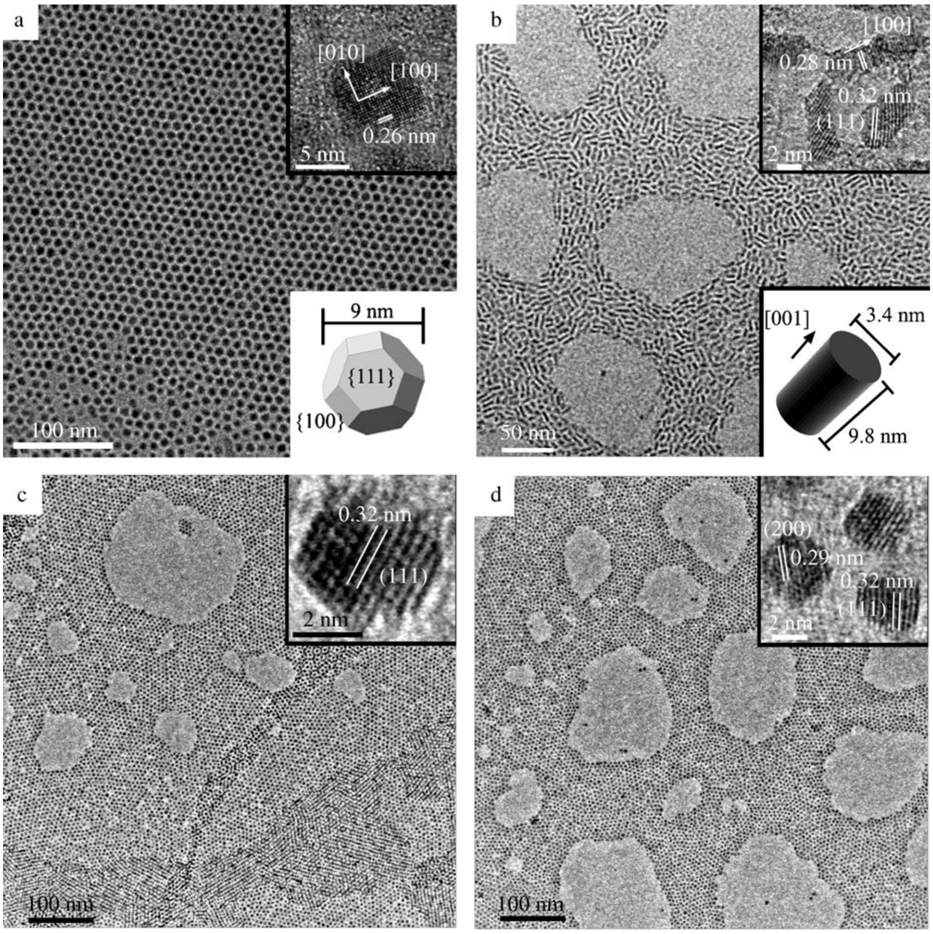

Figure 7. a) TEM and HRTEM (upper inset) images of LuOF nanopolyhedra, the lower inset shows a schematic diagram of a nanosized truncated-octahedron. b) TEM and HRTEM (upper inset) images of GdOF nanorods, the lower inset shows a schematic diagram of a nanorod. TEM and HRTEM (insets) images of c) SmOF and d) CeOF nanopolyhedra.

Phase control: The phase-selective synthesis of REOF and REF_3 nanocrystals was quite complicated in this work (Tables S1–S4). In OA/ODE, for the rare earths from La to Eu,

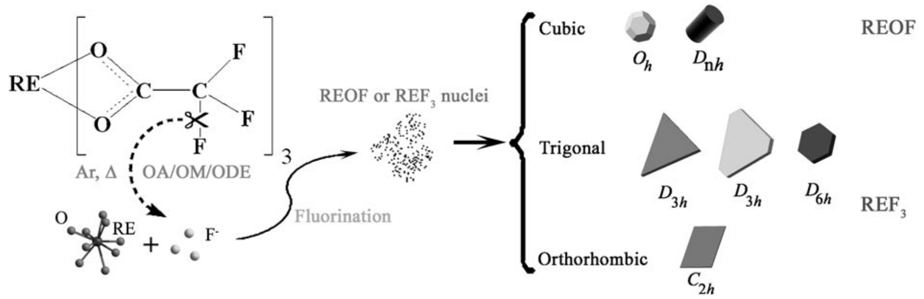

Scheme 1. Hypothesized mechanism for the formation of high-quality REOF and REF_3 nanocrystals from trifluoroacetate complex precursors through controlled fluorination in solution phase.

only trigonal REF_3 nanocrystals could be obtained, regardless of the synthetic conditions. However, the cases for those from Gd to Lu, including Y, were completely different, the phase compositions of the final products relied heavily on the synthetic parameters, together with the kind of rare earths we used. The nanoparticles of cubic REOF, trigonal REF_3, orthorhombic REF_3, or their mixtures might be yielded (as an example, see Table S3). The complexity of the phase control in OA/OM is similar to that in OA/ODE. In both cases, it was demonstrated that the phase control was highly sensitive to the reaction temperature and the solvent composition (ratios of OA/ODE and OA/OM). For example, by using 1 mmol [$Ho(CF_3COO)_3$] as the precursor, cubic HoOF nanopolyhedra of 6.1 ± 0.6 nm (Figure 8a,b) were obtained at 280 °C with OA/ODE = 1:1 after 1 h. Under this fixed OA/ODE ratio and reaction time, as the temperature was raised to 305 °C, trigonal HoF_3 polygonal nanoplates of 8.1 ± 0.9 nm were formed (Figure 8a and Figure S3c). The reaction at 320 °C produced relatively larger nanoparticles composed of a majority of orthorhombic HoF_3 nanoplates and a minority of cubic HoOF spherical nanoparticles (Figure 8a,c). The further elevated temperature of 335 °C yielded cubic HoOF nanospheres of 10.3 ± 1.5 nm (Figure 8a,d). The appearance of cubic HoOF again at higher temperatures might be due to the pyrohydrolysis of HoF_3, which could be further confirmed by the synthesis using 1 mmol orthorhombic HoF_3 nanocrystals as precursors. The reaction at 335 °C caused the orthorhombic HoF_3 nanocrystals to transform into cubic HoOF ones (Figure 8a). In fact, Barreca et al. found the hydrolytic transformation of LaF_3 into LaOF at temperatures above 250 °C in the chemical-vapor deposition (CVD) preparation of LaOF-based films from the [$La(hfa)_3$]·diglyme (Hhfa = 1,1,1,5,5,5-hexafluoro-2,4-pentanedione, diglyme = bis(2-methoxyethyl)ether) precursor.[15] The reappearance of cubic phase at elevated reaction temperature was frequently observed for the rare earths from Tb to Er during synthesis (Table S4). At the fixed reaction temperature of 320 °C and a reaction time of 1 h, the decrease in amount of OA from OA/ODE = 1:1 to 1:9 produced less

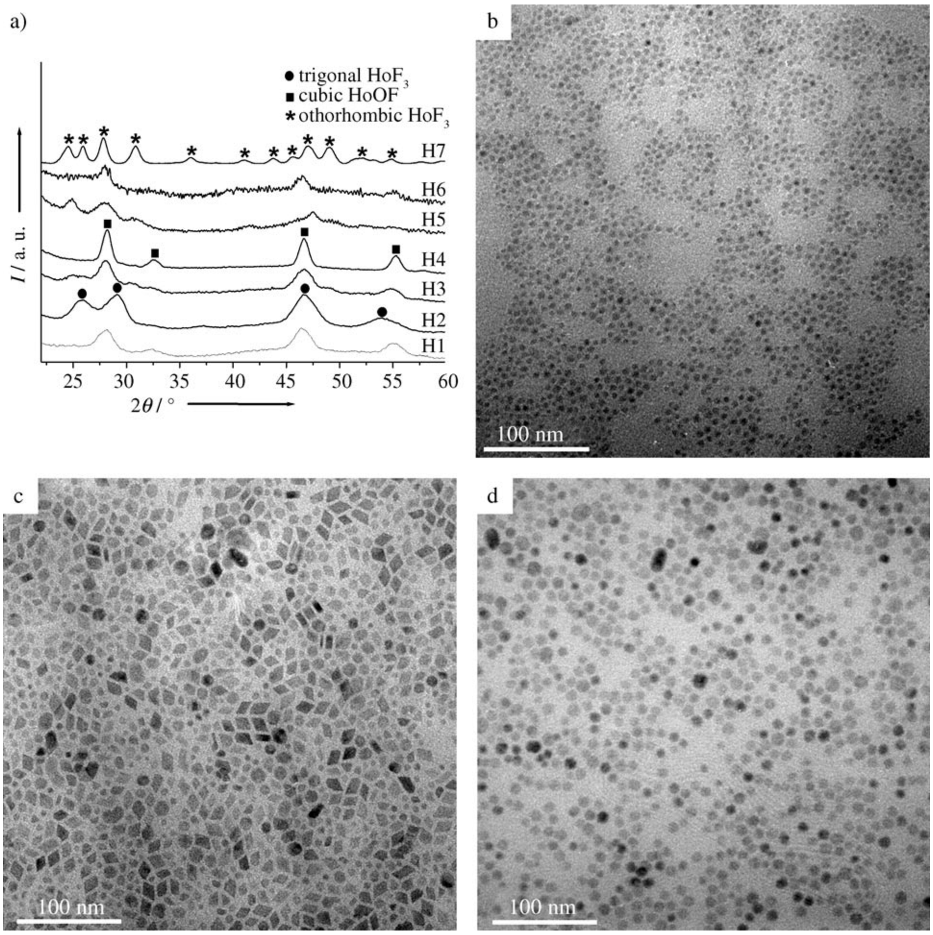

Figure 8. a) XRD patterns of some Ho samples, synthesized by using 1 mmol [$Ho(CF_3COO)_3$] as precursor (H1: 280 °C, OA/ODE = 1:1, 1 h; H2: 305 °C, OA/ODE = 1:1, 1 h; H3: 320 °C, OA/ODE = 1:1, 1 h; H4: 335 °C, OA/ODE = 1:1, 1 h; H5: 320 °C, OA/ODE = 1:9, 1 h; H6: 1 mmol H5, 335 °C, OA/ODE = 1:1, 1 h; H7: 320 °C, OA/ODE = 0:40, 1 h). b–d) TEM images of H1, H3, and H4, respectively.

well-shaped and poorly crystallized HoF_3 nanoplates (Figure 8a and Figure S12a). Furthermore, in pure ODE, severely aggregated and irregular orthorhombic HoF_3 nanoparticles were obtained (Figure 8a and Figure S12b).

To summarize, we could selectively synthesize high-quality cubic REOF, trigonal, or orthorhombic REF_3 nanocrystals by manipulating the reactivity of F^- ions, together with the coordination interactions between the nanocrystals and the coordinating surfactants of OA and OM, mainly through changing the solvent composition as well as the reaction temperature.

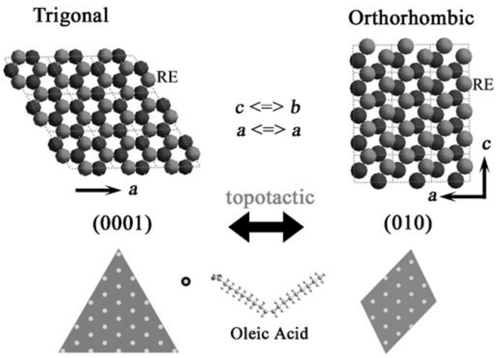

Scheme 2. Crystal structures of trigonal REF_3 viewed along the (0001) crystal plane and orthorhombic REF_3 viewed along the (010) crystal plane (the direction perpendicular to the nanoplates); the schematic arrangement of rare-earth cations and oleic acid ligands on the nanoplates. Oleic acid is assumed to be attached to the surface RE^{3+} ions.

Shape evolution and size control: The mechanism of shape-controlled synthesis of nanocrystals is currently receiving intensive investigation.[3] In the thermolysis of the complex precursors, capping ligand (variety, concentration, and selective adsorption onto particular crystallographic facets) plays a key role in the shape-control process. Condition-dependent experiments were carefully conducted to reveal the shape evolution of REF_3 and REOF nanocrystals across the rare-earth series. Considering the ultrathin thickness (1–3 nm) and the large ratio of the edge length to the thickness of our REF_3 nanoplates, we suggest that the adoption of a platelike shape for either trigonal or orthorhombic REF_3 nanocrystals should be a result of the selective adsorption of surfactants onto specific crystal planes (Scheme 2), as in the cases of the synthesis of Co and Cu_2S nanodisks,[4d,e] and rare-earth oxide nanoplates and nanodisks.[5b] Herein, we take the SmF_3 hexagonal nanoplate as an example to rationalize this hypothesis. At the fixed reaction temperature of 305 °C and the reaction time of 1 h, the increase in OA/ODE ratio from 1:1 to 4:1 led to an increase in edge length of the SmF_3 hexagonal nanoplates in trigonal structure (Figure 1 and Figure S13) from 12.7 ± 0.5 nm (Figure 3a and Table S1) to 13.7 ± 0.7 nm (Figure 9a,b). Simultaneously, the thickness of the nanoplates decreased slightly from 1.8 ± 0.2 nm (Table S1) to 1.7 ± 0.2 nm (Figure 9c). Therefore, the formation of trigonal REF_3 nanoplates (triangular, truncated-triangular, and hexagonal) should be attributed to the two-dimensional growth of the homogeneous REF_3 nuclei with the rigidly growth-blocked {0001} facets, related to the strong adsorp-

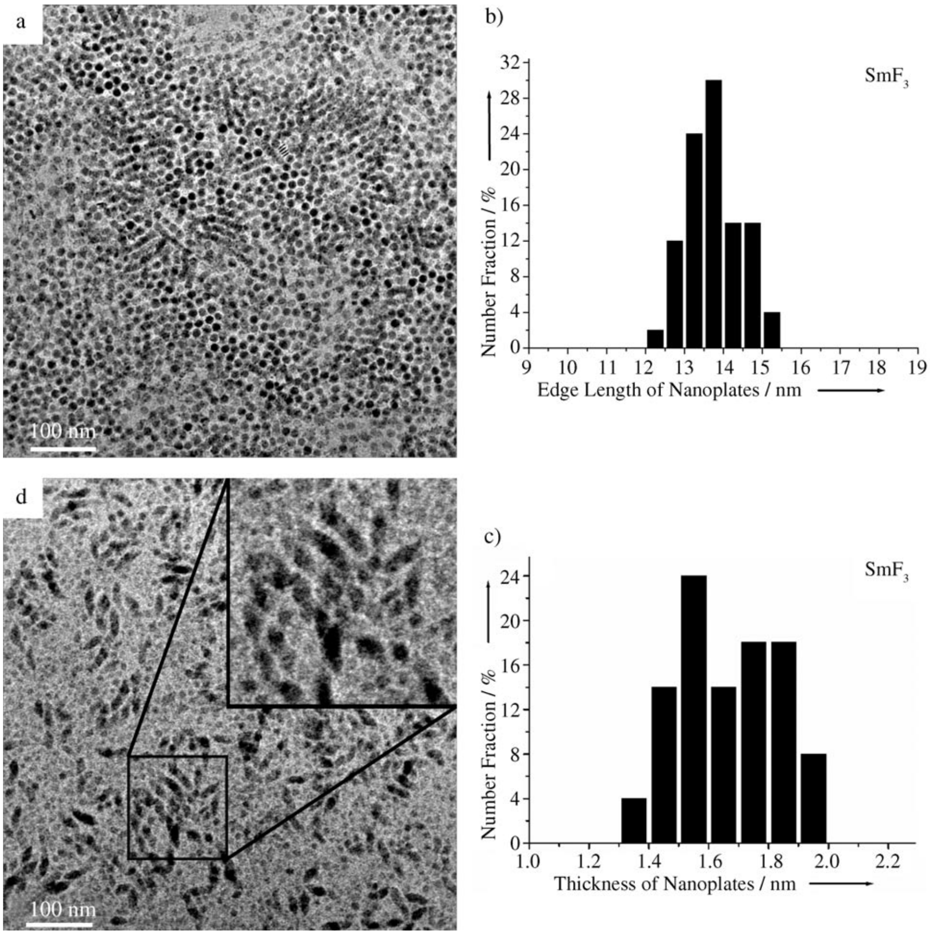

Figure 9. a) TEM image of SmF_3 hexagonal nanoplates synthesized at 305 °C with OA/ODE = 4:1 for 1 h. Distribution histograms of b) the edge length and c) thickness of the SmF_3 hexagonal nanoplates. d) TEM image of GdF_3 nanoplates synthesized at 310 °C with OA/ODE = 1:1 for 40 min (inset was taken from the highlighted square at high magnification).

tion of oleic acid onto them during nanocrystal growth. The selective adsorption suggested strong coordination between the surface rare-earth atoms on the (0001) crystal plane and the oleate ligands, which could refrain from the growth of this facet. Similarly, orthorhombic REF_3 quadrilateral nanoplates were formed through markedly restrained growth along the direction of [010], due to the topotactic relation between trigonal and orthorhombic structures (Scheme 2).[16] In fact, the arrangement of rare-earth cations on the (0001) crystal plane of the trigonal structure is quite similar to that on the (010) plane of the orthorhombic structure (Scheme 2 and Figure S9). It was also noted that an oriented aggregation could sometimes take place for the REF_3 quadrilateral nanoplates, forming zigzag-shaped nanoplates. For instance, nonuniform orthorhombic GdF_3 nanocrystals containing quadrilateral nanoplates, zigzag-shaped nanoplates, and small nanoparticles were formed from the reaction using $[Gd(CF_3COO)_3]$ as the precursor and OA/ODE at 310°C for 40 min (Figure S13 and Figure 9d). As the reaction time reached 1 h, uniform GdF_3 zigzag-shaped nanoplates were obtained (Figure 5a). This result clearly indicated the occurrence of the oriented aggregation of quadrilateral nanoplates into zigzag-shaped ones.[17] The estimated number of the primary particles is about four (see Figure 5b). As for the EuOF and GdOF nanocrystals, the rod-shape was formed with OA/OM = 5:3, whereas the polyhedral shape was formed with OA/OM = 3:5 (Table S2), suggesting that the weakest adsorption of oleate ligand on the (100) facet of the cubic structure should play a key role in the one-dimensional growth of the nanorods.

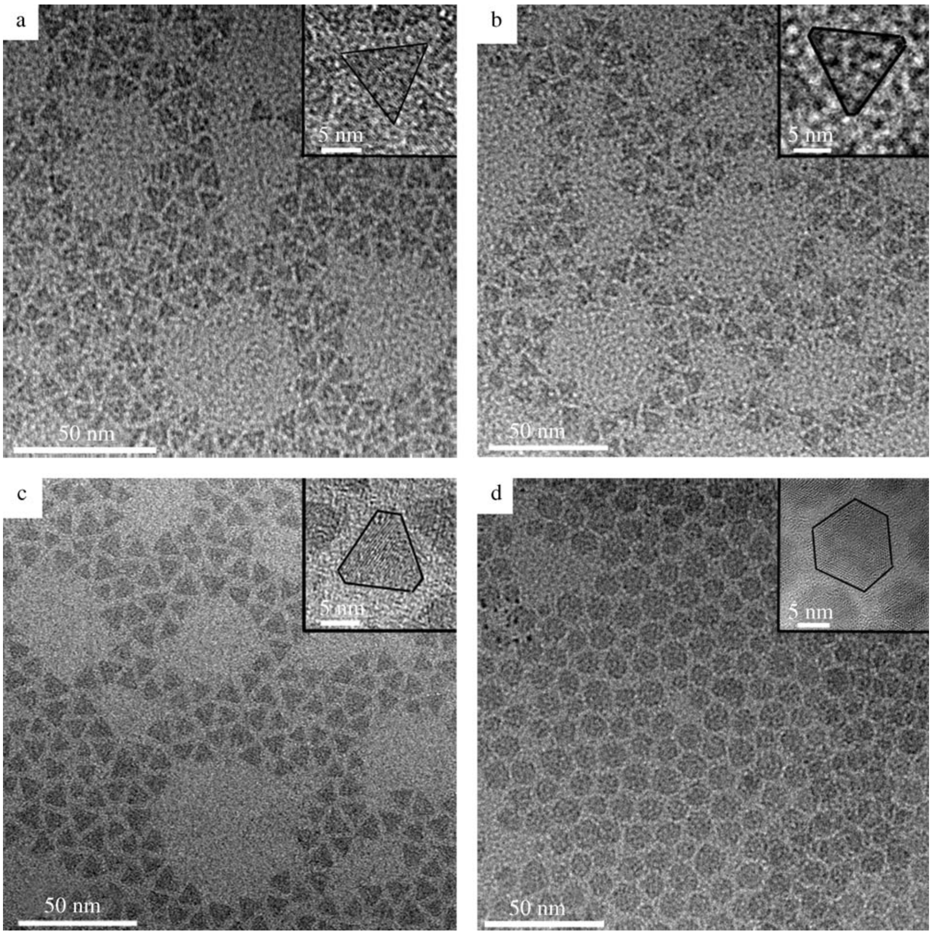

Figure 10. TEM images of LaF_3 nanoplates synthesized at 300°C with OA/ODE = 1:1 over a) 10 min, b) 20 min, c) 30 min, and d) 60 min.

Our further research strongly suggested that the triangular and truncated-triangular plate shapes for the trigonal REF_3 nanocrystals might be kinetically stable, whereas the hexagonal plate was likely to be the thermodynamically stable shape. Herein, we used the LaF_3 nanoplate as an example to support this deduction. Figure 10 shows the time-dependent shape evolution of LaF_3 nanoplates synthesized at 300°C with OA/ODE = 1:1. All the differently shaped LaF_3 nanoplates have the trigonal structure (Figure S14). After 10 min, triangular nanoplates of 9.0 nm (SD: 8.9%; Figure 10a and Figure S15a) were formed. After 20 min, the triangular nanoplates became slightly truncated, showing a slightly increased size of 10.6 nm (SD: 9.4%; Figure 10b and Figure S15b). After 30 min, the considerably truncated triangular nanoplates were obtained at a reduced size of 9.6 nm (SD: 10.4%; Figure 10c and Figure S15c). After 60 min, the truncated-triangular nanoplates had transformed into hexagonal ones with a continually decreased size of 9.1 nm, but showing a considerably broader size distribution (SD: 18.7%; Figure 10d and Figure S15d). Therefore, we considered that the observed time-dependent truncation should be due to the relatively high energy of the tips of the LaF_3 triangular nanoplates. As the truncation took place so as to reduce the total energy of the nanoplates, along with dissolution of the tips, the size defocusing occurred naturally, due to the Ostwald ripening process.[18] These results strongly suggest that for a given inorganic compound, differently shaped nanocrystals could be obtained by tuning the nanocrystal growth to the kinetic growth region or thermodynamic growth region.

The size of nanocrystals obtained can be easily tuned by changing the concentration of the precursors, reaction temperature, and reaction time. For instance, by using 1 mmol

[Eu(CF_3COO)$_3$] in OA/ODE = 1:1 for a reaction at 305 °C for 60 min, we obtained EuF_3 hexagonal nanoplates with an edge length of 11.5 ± 1.0 nm (Figure 3g). Also at 305 °C, but by decreasing the [Eu(CF_3COO)$_3$] concentration to 0.5 mmol and the reaction time to 0.5 h, smaller nanoplates (8.5 ± 1.2 nm) were produced. Furthermore, with a reaction time of 0.5 h, an increased [Eu(CF_3COO)$_3$] concentration to 2 mmol, and an increased reaction temperature of 315 °C, we obtained larger crystals (14.0 ± 1.3 nm).

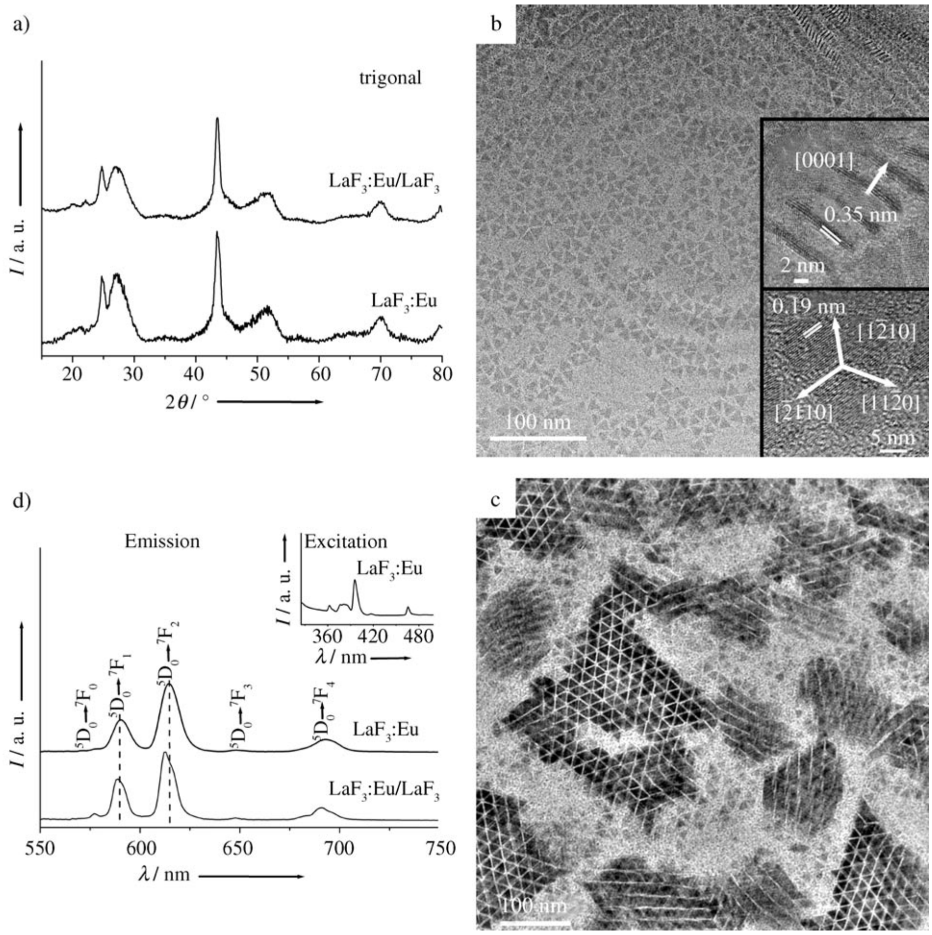

Figure 11. a) XRD patterns of LaF_3:5 % Eu and LaF_3:5 % Eu/LaF_3 triangular nanoplates. TEM images of LaF_3: b) 5 % Eu and c) LaF_3:5 % Eu/LaF_3 triangular nanoplates. d) Room-temperature fluorescence emission spectra of LaF_3:5 % Eu and LaF_3:5 % Eu/LaF_3 triangular nanoplates (λ_{em} = 396 nm) dispersed in hexane/toluene (1:1) at 0.05 mol L^{-1}, inset is the excitation spectrum of LaF_3:5 % Eu triangular nanoplates (λ_{em} = 614 nm).

Optical properties of LaF_3:5 % Eu and LaF_3:5 % Eu/LaF_3 nanocrystals: LaF_3 is a well-known, ideal host material for various phosphors because of the minimal quenching of the excited state of the rare-earth ions resulting from its very low phonon energy. By using the SSP approach developed, we could also obtain high-quality composite rare-earth fluoride nanocrystals, with multiple rare-earth trifluoroacetates as the precursors. Figure 11a depicts the XRD patterns of the LaF_3:5 % Eu and LaF_3:5 % Eu/LaF_3 samples synthesized with OA/ODE = 1:1 at 300 °C for 30 min. Both samples appear to have a pure trigonal structure. The calculated lattice parameters are a = 7.194 and c = 7.224 Å for the LaF_3:5 % Eu nanocrystals, which are smaller than those of the LaF_3 triangular nanoplates (a = 7.232 and c = 7.285 Å),[9c] indicating that Eu^{3+} cations were well doped into the LaF_3 lattice, with the formation of a $La_{0.95}Eu_{0.05}F_3$ solid solution in this case. The calculated lattice parameters are a = 7.20 and c = 7.23 Å for the LaF_3:5 % Eu/LaF_3 nanocrystals, which lie between those of LaF_3 and LaF_3:5 % Eu nanocrystals, suggesting that a LaF_3 layer was possibly coated onto the surfaces of the LaF_3:5 % Eu nanocrystals. TEM characterization revealed that we obtained LaF_3:5 % Eu triangular nanoplates of (1.5 ± 0.2) nm × (13.0 ± 1.2) nm (Figure 11b). Figure 11c shows that the LaF_3:5 % Eu/LaF_3 sample is composed of highly uniform triangular nanoplates of size (1.6 ± 0.1) nm × (16.3 ± 0.8) nm. Compared with the LaF_3:5 % Eu nanoplates, the LaF_3:5 % Eu/LaF_3 ones showed a remarkable increase in edge length from 13.0 to 16.3 nm, along with a nearly unchanged thickness. Under these conditions, the Eu atoms on the side surfaces might be covered by the LaF_3 layer (ca. 1 nm in thickness), whereas those on the top and bottom surfaces were nearly unchanged (Figure 11b,c). As a result, the coating of the LaF_3 layer decreased the surface Eu atoms for the LaF_3:5 % Eu nanoplates by approximately 30 %, as estimated from the surface-area variation.

Figure 11d shows the room-temperature emission spectra of the as-obtained LaF_3:5 % Eu and LaF_3:5 % Eu/LaF_3 nanoplates redispersed in toluene/hexane (1:1). The spectra are characteristic of the $^5D_0 \to {}^7F_J$ line emissions (J = 0, 1, 2, 3, 4) of the Eu^{3+} ion. Notably, the ratio of the $^5D_0 \to {}^7F_2$ to $^5D_0 \to {}^7F_1$ transition (I_{614}/I_{590}), known as the asymmetric ratio, is 2.22 for the LaF_3:5 % Eu nanoplates and 1.65 for the LaF_3:5 % Eu/LaF_3 nanoplates, suggesting the presence of a strong surface effect on the red emission of the oleate-capped nanocrystals relative to the bulk counterpart.[9d] As is well known, the $^5D_0 \to {}^7F_2$ transition is electric-dipole allowed, while the $^5D_0 \to {}^7F_1$ transition is magnetic-dipole allowed.[9d,19] Consequently, the intensity of the $^5D_0 \to {}^7F_2$ transition is much more sensitive to the symmetry in local environments around Eu^{3+} ions than that of the $^5D_0 \to {}^7F_1$ transition. The less symmetric the local environment around Eu^{3+} ions, the higher the probability of the $^5D_0 \rightarrow {}^7F_2$ transition, and, thus, the stronger the $^5D_0 \rightarrow {}^7F_2$ emission. Generally, the surface atoms have a lower coordination number, and, thus, lower symmetry than the bulk atoms. Therefore, the values of I_{614}/I_{590} for our nanoplates are considerably larger than that of the bulk counterpart, showing a strong surface effect resulting from their higher fractions of surface Eu atoms.[9d] With the coating of the LaF_3 layer onto the side surfaces of the LaF_3:5%Eu nanoplates, the surface effect was markedly weakened due to the reduced fraction of surface Eu atoms. Consequently, the ratio of I_{614}/I_{590} decreased from 2.22 for the LaF_3:5%Eu nanoplates to 1.65 for the LaF_3:5%Eu/LaF_3 nanoplates.

Conclusions

High-quality REF_3 and REOF nanocrystals with diverse shapes (trigonal REF_3 triangular, truncated-triangular, hexagonal, and polygonal nanoplates; orthorhombic REF_3 quadrilateral and zigzag-shaped nanoplates; cubic REOF nanopolyhedra and nanorods) were synthesized by using $[RE(CF_3COO)_3]$ as precursors through the controlled fluorination in oleic acid/oleylamine/1-octadecene. The combination of rare-earth, oxygen, and fluorine atoms in $[RE(CF_3COO)_3]$ (namely SSP) allowed the selective preparation of REF_3 and REOF compounds through reorganization of the bond from RE−O to RE−F at the nucleation stage in the solution phase. By tuning the polarity of the dispersant along with the nanocrystal concentration, we could align those nanocrystals with diverse geometric symmetries (such as D_{3h}, D_{6h}, C_{2h}, O_h, and D_{nh}) to form highly ordered nanoarrays on a large area of the copper TEM grids by self-assembly. Particularly, the plate-shaped REF_3 nanocrystals could form highly ordered nanoarrays in either the face-to-face formation or the edge-to-edge formation. By carefully modifying synthetic parameters, such as solvent composition, reaction temperature, and reaction time, we could manipulate the phase, shape, and size of these nanocrystals. A selective adsorption of capping ligands onto specific crystal planes of the nanocrystals was assumed to account for the two-dimensional growth of the trigonal and orthorhombic REF_3 nanoplates, and for the one-dimensional growth of cubic REOF nanorods. This SSP synthetic strategy could be readily scaled up to gram-grade production of the nanocrystals, and also enabled the preparation of high-quality LaF_3:Eu and LaF_3:Eu/LaF_3 triangular nanoplates, demonstrating its robustness and versatility. As the LaF_3 layer was coated onto the side surfaces of the LaF_3:Eu nanoplates, the red emission of Eu^{3+} ions in LaF_3:Eu due to the surface effect was remarkably reduced, indicating that Eu^{3+} ions could serve as a sensitive structure probe to detect the lattice symmetry of the host materials.[20] We expect that the differently shaped rare-earth fluoride and oxyfluoride nanocrystals obtained, including the luminescent ones, could serve as powerful nanobuilding blocks for constructing new self-organized superlattices (such as binary nanoparticle superlattices,[2b] in conjunction with semiconductor or noble-metal colloidal nanocrystals) of current interest, and future self-assembled nanodevices.[2] Our further research will focus on the self-assembly principles and optical properties of the nanocrystals obtained, as well as extension of the method described towards the synthesis of MF_x (M: alkaline-earth metal and transitional metal) nanocrystals.

This work may represent a new and significant step in the study of nanostructured fluoride materials, and should enrich the fields of lanthanide and fluoride chemistry to promote the size-/shape-/phase-control theory and self-assembly principles for dispersible nanocrystals, to facilitate the fabrication of advanced rare-earth functional materials with excellent applications, and to advance development of synthetic methodologies for colloidal, inorganic nanocrystals.

Experimental Section

Chemicals: Oleic acid (OA; 90%, Alpha), oleylamine (OM;>80%, Acros), 1-octadecene (ODE;>90%, Acros), absolute ethanol, hexane, and toluene were used as received. $[RE(CF_3COO)_3]$ precursors were prepared according to a literature method[11] by using rare-earth oxides (>99.95%) and trifluoroacetic acid (99%, Acros) as starting materials.

Nanocrystal synthesis

All nanocrystals were synthesized by using standard oxygen-free procedures.

Synthesis of REF_3 and REOF nanocrystals: A typical procedure: A given amount of $[RE(CF_3COO)_3]$ (1 mmol) was added into 40 mmol of OA/OM/ODE (Tables S1 and S2) in a three-necked flask (100 mL) at RT. The slurry was heated to 100 °C with vigorous magnetic stirring under vacuum for several minutes in a temperature-controlled electromantle to remove water and oxygen, thereby forming an optically transparent solution. The solution was then heated to a temperature between 280 and 335 °C at a heating rate of 18 °C min^{-1} and maintained for 1 h under an Ar atmosphere. On cooling to RT, the nanocrystals were precipitated by adding an excess of a hexane/ethanol mixture (v/v = 1:4) into the reaction solution, followed by washing with ethanol and drying in air at 60 °C. The as-prepared nanocrystals could be easily redispersed in various nonpolar organic solvents, such as hexane and toluene. The yields of all nanocrystals obtained were 65–75%.

Synthesis of LaF_3:5%Eu nanocrystals: The synthetic procedure was the same as that used to synthesize LaF_3 nanocrystals, except that 0.95 mmol $[La(CF_3COO)_3]$ and 0.05 mmol $[Eu(CF_3COO)_3]$ were taken as the precursors, and were added into a mixture of OA (20 mmol) and ODE (20 mmol) in a three-necked flask at RT for reaction at 300 °C for 30 min.

Synthesis of LaF_3:5%Eu/LaF_3 nanocrystals: The synthetic procedure was the same as that used to synthesize LaF_3:5%Eu nanocrystals, except that 1 mmol LaF_3:5%Eu nanocrystals and 0.67 mmol $[La(CF_3COO)_3]$ were taken as the precursors, and were added into a mixture of OA (20 mmol) and ODE (20 mmol) in a three-necked flask at RT.

Characterization: Samples for XRD analysis were prepared by drying the nanocrystals in an oven at 60 °C for 12 h. The XRD patterns were recorded by using a Rigaku D/MAX-2000 diffractometer with a slit of 0.5° at a scanning rate of 2° min^{-1} using $Cu_{K\alpha}$ radiation ($\lambda = 1.5406$ Å). The lattice parameters were calculated by using the least-squares method. Samples for transmission electron microscopy (TEM) analysis were prepared by drying a dispersion of the nanocrystals on amorphous carbon-coated copper grids. TEM and high-resolution TEM (HRTEM) micrographs were obtained by using a Philips Tecnai F30 FEG-TEM operated at 300 kV. RT photoluminescent fluorescence spectra of LaF_3:5%Eu and

LaF_3:5 %Eu/LaF_3 nanocrystals were measured by using a Hitachi F-4500 spectrophotometer equipped with a 150-W Xe-arc lamp at a fixed band-pass of 0.2 nm and constant instrument parameters (5.0 nm for excitation split, 2.5 nm for emission split, and 700 V for PMT voltage), with the nanocrystal dispersions in a mixture of toluene/hexane (v/v = 1:1) at a concentration of 0.05 mol$\,L^{-1}$.

Acknowledgements

We gratefully acknowledge financial aids from the MOST of China (Grant No. 2006CB601104) and the NSFC (Grant Nos. 20571003, 20221101, and 20423005).

---

[1] a) L. E. Brus, *J. Chem. Phys.* **1984**, *80*, 4403; b) C. B. Murray, D. J. Norris, M. G. Bawendi, *J. Am. Chem. Soc.* **1993**, *115*, 8706; c) A. P. Alivisatos, *Science* **1996**, *271*, 933; d) T. S. Ahmadi, Z. L. Wang, T. C. Green, A. Henglein, M. A. El-Sayed, *Science* **1996**, *272*, 1924; e) M. Bruchez, Jr., M. Moronne, P. Gin, S. Weiss, A. P. Alivisatos, *Science* **1998**, *281*, 2013; f) S. Sun, C. B. Murray, D. Weller, L. Folks, A. Moser, *Science* **2000**, *287*, 1989.

[2] a) E. Rabani, D. R. Reichman, P. L. Geissler, L. E. Brus, *Nature* **2003**, *426*, 271; b) E. V. Shevchenko, D. V. Talapin, N. A. Kotov, S. O'Brien, C. B. Murray, *Nature* **2006**, *439*, 55; c) E. V. Shevchenko, D. V. Talapin, C. B. Murray, S. O'Brien, *J. Am. Chem. Soc.* **2006**, *128*, 3620; d) J. Cheon, J. Park, J. Choi, Y. Jun, S. Kim, M. G. Kim. , Y. J. Kim, *Proc. Natl. Acad. Sci. USA* **2006**, *103*, 3023; e) B. Liu, H. C. Zeng, *J. Am. Chem. Soc., 127*, 18262.

[3] Recent reviews related to the synthesis of colloidal nanocrystals: a) Y. Yin, A. P. Alivisatos, *Nature* **2005**, *437*, 664; b) Y. Jun, J. Lee, J. Choi, J. Cheon, *J. Phys. Chem. B* **2005**, *109*, 14795.

[4] a) X. Peng, L. Manna, W. Yang, J. Wickham, E. Scher, A. Kadavanich, A. P. Alivisatos, *Nature* **2000**, *404*, 59; b) M. A. Malik, N. Revaprasadu, P. O'Brien, *Chem. Mater.* **2001**, *13*, 913; c) W. W. Yu, X. Peng, *Angew. Chem.* **2002**, *114*, 2474; *Angew. Chem. Int. Ed.* **2002**, *41*, 2368; d) V. F. Puntes, D. Zanchet, C. K. Erdonmez, A. P. Alivisatos, *J. Am. Chem. Soc.* **2002**, *124*, 12874; e) M. B. Sigman, Jr., A. Ghezelbash, T. Hanrath, A. E. Saunders, F. Lee, B. A. Korgel, *J. Am. Chem. Soc.* **2003**, *125*, 16050; f) E. V. Shevchenko, D. V. Talapin, H. Schnablegger, A. Kornowski, O. Festin, P. Svedlindh, M. Haase, H. Weller, *J. Am. Chem. Soc.* **2003**, *125*, 9090; g) J. Park, K. An, Y. Hwang, J.-G. Park, H.-J. Noh, J.-Y. Kim, J.-H. Park, N.-M. Hwang, T. Hyeon, *Nat. Mater.* **2004**, *3*, 891; h) W. S. Seo, J. H. Shim, S. J. Oh, E. K. Lee, N. H. Hur, J. T. Park, *J. Am. Chem. Soc.* **2005**, *127*, 6188; i) B. D. Yuhas, D. O. Zitoun, P. J. Pauzauskie, R. He, P. Yang, *Angew. Chem.* **2006**, *118*, 434; *Angew. Chem. Int. Ed.* **2006**, *45*, 420.

[5] a) R. Si, Y.-W. Zhang, L.-P. You, C.-H. Yan, *Angew. Chem.* **2005**, *117*, 3320; *Angew. Chem. Int. Ed.* **2005**, *44*, 3256; b) T. Yu, J. Joo, Y. I. Park, T. Hyeon, *J. Am. Chem. Soc.* **2006**, *128*, 1786.

[6] O. Lehmann, K. Kömpe, M. Haase, *J. Am. Chem. Soc.* **2004**, *126*, 14935.

[7] J. W. Stouwdam, M. Raudsepp, F. C. J. M. van Veggel, *Langmuir* **2005**, *21*, 7003.

[8] F. Zhao, H. L. Sun, G. Su, S. Gao, *Small* **2006**, *2*, 244.

[9] a) J. W. Stouwdam, F. C. J. M. van Veggel, *Nano. Lett.* **2002**, *2*, 733; b) S. Heer, K. Kömpe, H.-U. Güdel, M. Haase, *Adv. Mater.* **2004**, *16*, 2102; c) Y.-W. Zhang, X. Sun, R. Si, L.-P. You, C.-H. Yan, *J. Am. Chem. Soc.* **2005**, *127*, 3260; d) V. Sudarsan, F. C. J. M. van Veggel, R. A. Herring, M. Raudsepp, *J. Mater. Chem.* **2005**, *15*, 1332; e) X. Wang, J. Zhuang, Q. Peng, Y. Li, *Nature* **2005**, *437*, 121; f) J.-L. Lemyre, A. M. Ritcey, *Chem. Mater.* **2005**, *17*, 3040; g) P. R. Diamente, F. C. J. M. van Veggel, *J. Fluoresc.* **2005**, *15*, 543; h) F. Wang, Y. Zhang, X. Fan, M. Wang, *J. Mater. Chem.* **2006**, *16*, 1031; i) Z. L. Wang, Z. W. Quan, P. Y. Jia, C. K. Lin, Y. Luo, Y. Chen, J. Fang, W. Zhou, C. J. O'Connor, J. Lin, *Chem. Mater.* **2006**, *18*, 2030; j) F. Evanics, P. R. Diamente, F. C. J. M. van Veggel, G. J. Stanisz, R. S. Prosser, *Chem. Mater.* **2006**, *18*, 2499; k) H.-X. Mai, Y.-W. Zhang, R. Si, Z.-G. Yan, L.-D. Sun, L.-P. You, C.-H. Yan, *J. Am. Chem. Soc.* **2006**, *128*, 6426.

[10] J. Lee, Q. Zhang, F. Saito, *J. Alloys Compd.* **2003**, *348*, 214.

[11] J. E. Roberts, *J. Am. Chem. Soc.* **1961**, *83*, 1087.

[12] a) A. Zalkin, D. H. Templeton, *J. Am. Chem. Soc.* **1953**, *75*, 2453; b) R. E. Thoma, G. D. Brunton, *Inorg. Chem.* **1966**, *5*, 1937.

[13] J.-H. Müller, T. Petzel, *J. Alloys Compd.* **1995**, *224*, 18.

[14] A. L. Willis, N. J. Turro, S. O'Brien, *Chem. Mater.* **2005**, *17*, 5970.

[15] D. Barreca, A. Gasparotto, C. Maragno, E. Tondello, E. Bontempi, L. E. Depero, C. Sada, *Chem. Vap. Deposition* **2005**, *11*, 426.

[16] K. Rotereau, Ph. Daniel, A. Desert, J. Y. Gesland, *J. Phys. Condens. Matter* **1998**, *10*, 1431.

[17] a) R. L. Penn, J. F. Banfield, *Science* **1998**, *281*, 969; b) R. L. Penn, *J. Phys. Chem. B* **2004**, *108*, 12707.

[18] Z. A. Peng, X. Peng, *J. Am. Chem. Soc.* **2001**, *123*, 1389.

[19] B. R. Judd, *Phys. Rev.* **1962**, *127*, 750.

[20] C.-H. Yan, L.-D. Sun, C.-S. Liao, Y.-X. Zhang, Y.-Q. Lu, S.-H. Huang, S.-Z. Lu, *Appl. Phys. Lett.* **2003**, *82*, 3511.

Received: July 24, 2006